Geophysica (1983), Vol. 20, No. 1, pp. 51–69
Printed in Finland

551.511:551.509:551.55

SURFACE WIND PREDICTIONS AND BOUNDARY LAYER MASS FLOW

by

SYLVAIN M. JOFFRE

Institute of Marine Research
P.B. 33, 00931 Helsinki 93, Finland

Abstract

A simple dynamical-statistical prediction model for surface wind over the Bothnian Bay is presented. Since thermal stability is difficult to obtain from routine observations, even though it is the main ingredient shaping wind profiles close to the surface, the main goal of this study was to incorporate it implicitly. The statistical relationships between the observed upper flow quantities and the surface flow or surface drag obtained from a field experiment suggest the use of a new wind concept predictor: the vertically averaged mean wind. Comparison with data gives encouraging results and calls for extension of the method. On the other hand, the mismatch of the predictions implies some future improvements.

1. *Introduction*

Knowledge of the wind over sea areas is of great importance for many activities. Unfortunately, offshore observations are very scarce. Furthermore, coastal wind observations are not representative because of the heterogeneity of the site during onshore wind while these observations represent only continental-like values during offshore wind situations.

Thus, numerical predictions are necessary with a more or less sophisticated model the starting point generally being a large-scale wind obtained either from pressure field observations or from a general circulation model. Accurate predictions would require detailed modelling of the atmospheric boundary layer (ABL) structure taking into account roughness features, stability, baroclinicity etc.. However, in certain circumstances, running an additional model for the purpose of a more

specific routine (*e.g.* wind wave predictions, ice-drift modelling) would be too painstaking and therefore statistical-dynamical predictions might be more relevant. Nevertheless, the various factors mentioned above (mainly thermal stability) should be incorporated, if not explicitly, then at least implicitly.

This is the basis of this paper which, starting from some wind statistics over the Northern Baltic Sea, proceeds to deduce some wind prediction schemes and finally to present some potential applications.

2. *The data*

In early spring 1977, a field experiment over the ice fields of the Bay of Bothnia (see Fig. 1) was carried out with mast measurements of wind and tem-

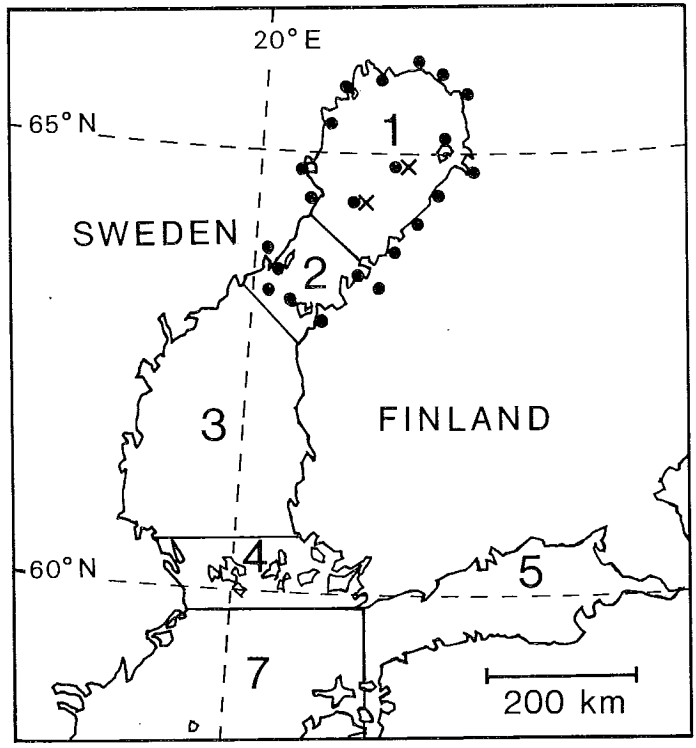

Fig. 1. Location of the two field sites (crosses) and the marine areas of the Northern Baltic Sea: (1) Bothnian Bay, (2) the Quark, (3) Bothnian Sea, (4) Aaland Sea and Archipelago, (5) Gulf of Finland, (7) Northern Baltic. The dots represent barograph locations during the experiment.

perature at five levels between one and 10 metres while pibal and radiosoundings provided wind, temperature and moisture profiles for the lowest layers of the atmosphere (up to a minimum of 500 m and an average of 2 km) (see JOFFRE, 1981). The mast anemometer outputs were 10 min-average values. In the present study, three consecutive runs were averaged providing 30-min-average values which are flagged by the ending time of the half hour to which they apply.

One important point in the study of the ABL structure is to establish the larger-scale flow in which the ABL flow is embedded. This was done using the pressure field analysed by the Finnish Meteorological Institute (FMI) on a 9x15 grid over northern Europe with a grid mesh of 150 km. The surface geostrophic wind V_{g0} was then computed with a second-order surface regression fit. A second estimate V_{ms} of the geostrophic wind was given using 21 barometric stations along the coast surrounding regions 1 and 2 of Fig. 1 and with one additional barograph at the experimental site in the centre of the region. Here, too, a second-order surface regression fit was applied providing a mesoscale estimate of the

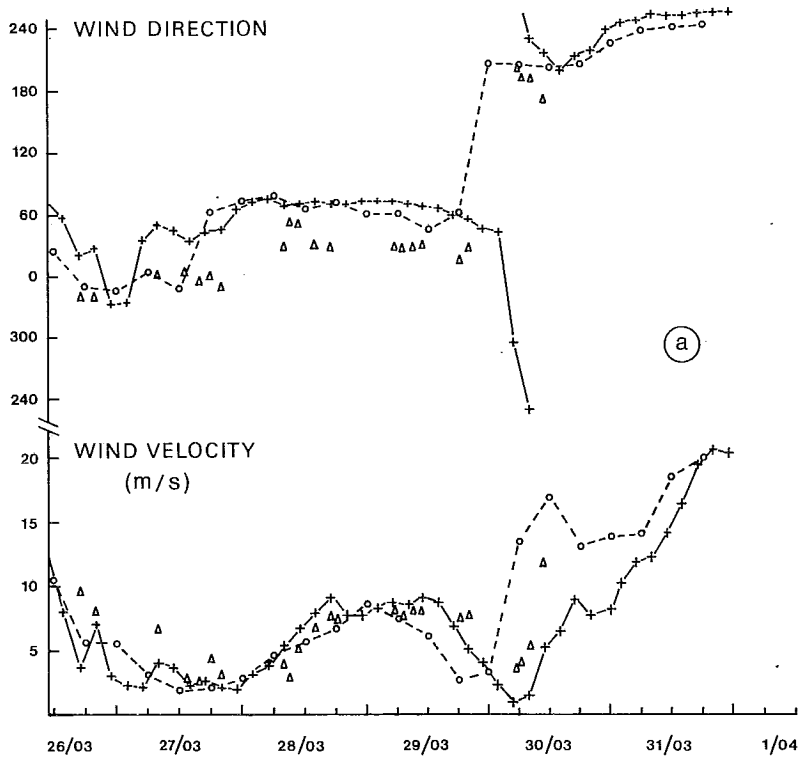

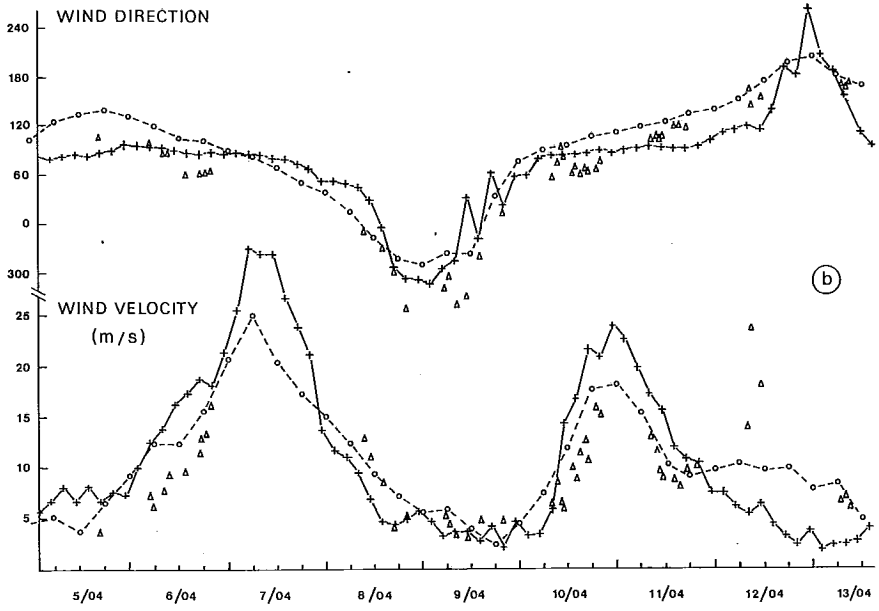

Fig. 2. Comparison of geostrophic wind vector modulus and direction computed either from surface pressure field analysis (open circles) or from a second-order surface fitting of a mesoscale pressure network (crosses) with actual upper wind observations at z = 500 m (triangles) for a) the F1 period, b) the F2 period.

forcing flow. These two (synoptic and mesoscale) geostrophic winds are compared with the observed wind at z = 500 m during the two experimental periods (Figs. 2). Note the departure, which may sometimes be large, between these different wind concepts. This stresses the difficulty of choosing the suitable external driving flow. The observed upper wind has sometimes been taken as an alternative to the geostrophic wind on the assumption that it contains part of the unstationarity and advective effects inherent in planetary flows. However, especially under baroclinic conditions, the value of the upper wind is very sensitive to the choice of the appropriate level. Moreover, upper wind determined from balloon profiles can fluctuate considerably and small errors in observed angles can give rise to sharp departures in the computed wind values.

3. *The ratio between surface and upper wind*

3.1 Empirical results

The basic effect of the earth's surface (rigid or fluid) is to retrieve momentum from the planetary atmospheric flow. The ABL is the only region acting as a momentum sink for the atmospheric flow. This adjustment of the upper free stream to surface conditions is modulated by the type of surface roughness and especially by the vertical temperature distribution. It has long been a matter of interest to relate this upper wind to the surface stress τ_0 or to the surface wind and to compare the direction of the upper flow (or geostrophic flow) with the surface flow direction (*cf.* Fig. 3). Such data or theories are generally represented by a function of the Rossby number $Ro = |V_{g0}|/fz_0$, which includes all the relevant external parameters (f is the Coriolis parameter and z_0 the roughness length). The dependence on thermal stability is superimposed on graphs of this type (see *e.g.* MONIN & YAGLOM, 1971, p. 410). Unfortunately, the scatter tends to be large.

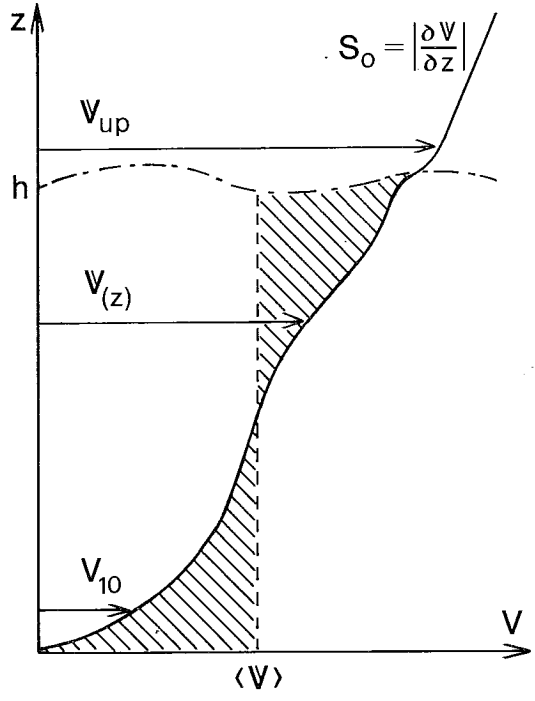

Fig. 3. Schematic representation of wind concepts.

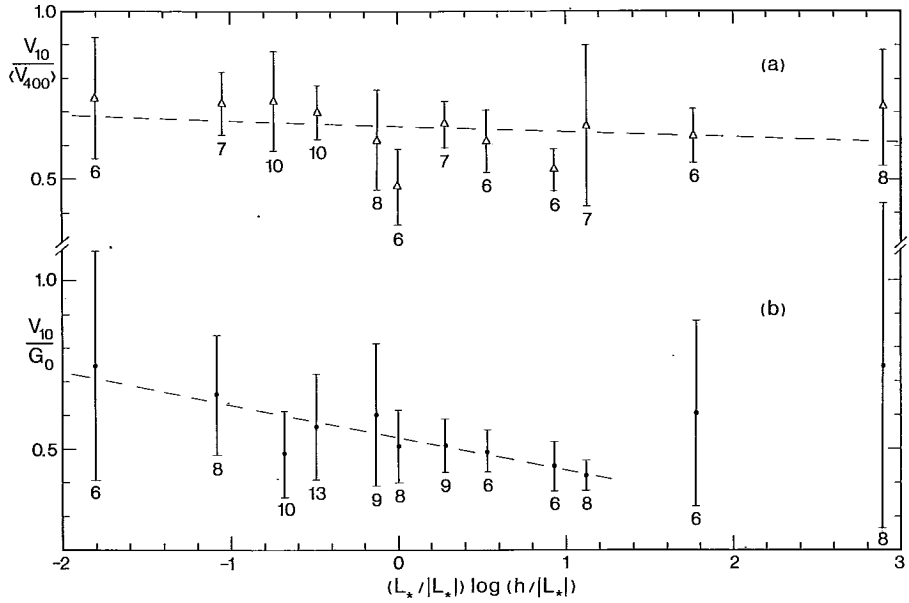

Fig. 4. Dependence on stability of a) the ratio $V_{10}/\langle V_{400}\rangle$ and b) V_{10}/G_0. The figures refer to the number of observations included in each mean value. One standard deviation is illustrated on each side of the mean.

In the present context we are interested in extracting a surface wind value from a given upper or geostrophic wind. The simplest way is to relate these two wind concepts through their ratio,

$$R = V_s/V_{up} \tag{1}$$

with, say, $V_s = V(z = 10\text{ m})$ and $V_{up} = |V_{g0}|$ or $V(z=h)$, where h is the height of the ABL. Assessment of h without upper turbulence measurements or sodar data is a very subjective operation. To avoid adding the uncertainty in h into our wind statistics, we took a fixed $h = 400$ m corresponding to the upper bound for the h values analysed (JOFFRE, 1981).

The dependence of the ratios V_{10}/G_0 (with $G_0 = |V_{g0}|$) and $V_{10}/\langle V_{400}\rangle$ on thermal stability is shown in Figs. 4a and 4b. The notation $\langle . \rangle$ refers to vertically integrated quantities throughout the ABL

$$\langle V\rangle = \frac{1}{h}\int_0^h V(z)\,dz$$

The stability parameter is $\mu_h = h/L_\star$ (*i.e.* proportional to $L_\star^{-1}$) with $L_\star$, the so-called Monin-Obukhov length, determined from turbulent fluxes of momentum and heat at the surface. The latter were determined by the profile method from our surface layer observations (JOFFRE, 1982).

The relevance of the quantity $\langle V_{400} \rangle$, compared with V_{400}, for instance, will be apparent later on. Note the larger scatter of the ratio with G_0 and the stronger dependence of the same quantity on stability. The marked scatter in very stable situations is due to both fluctuations in the weak surface wind and a mismatch between the 400 m-level and the real ABL height. In such cases the presence of a low-level jet with strong shear makes the choice of the reference level primordial for determining the ratio R.

However, the value of this ratio is affected by the non-included effect of baroclinicity and the unsteadiness of the flow in addition to the degree of horizontal resolution and the analysis techniques employed in the determination of G_0. Note that the level $z = 400$ m corresponds, on the average, to the standard 950 mb surface.

Since the surface wind is by no means always the final goal, but the surface stress τ_0 is required rather for oceanic circulation, ice drift or wind wave models, another alternative is to relate the upper or large-scale wind directly to the friction velocity $u_\star = (\tau_0/\rho_0)^{1/2}$, with ρ_0 air density, through the geostrophic drag coefficient (LETTAU, 1959):

$$C_g = (u_\star/V_{up})^2 \tag{2}$$

The dependence of C_g on thermal stability is illustrated in Figs. 5 and 6 for $V_{up} = \langle V_{400} \rangle$ and $V_{up} = G_0$, respectively. There is a general decrease from unstable to stable cases with a sudden fall off when $h/L_\star \gtrsim 20$–30. Here, too, the decrease is gentler and the scatter smaller in the former case with $\langle V_{400} \rangle$. The departure of the neutral values from the general trend might be due to some composite profiles obtained under transitional unsteady conditions. The lines drawn in these figures are eye best-fits. Note also that the scatter in C_g is much larger than in the R values.

However, once V_s has been determined, for instance through R, it must be related to τ_0 (or $u_\star$) through a drag coefficient C_D referring to the same height as V_s (generally 10 m). This coefficient C_D is known to be strongly dependent on thermal stability (JOFFRE, 1982) and also to have a larger scatter than C_g owing to nonlocal effects. This stability effect on C_D can be almost completely suppressed by lowering the reference height of the surface wind so as to be well within the dynamical sublayer where the Monin-Obukhov length is not supposed

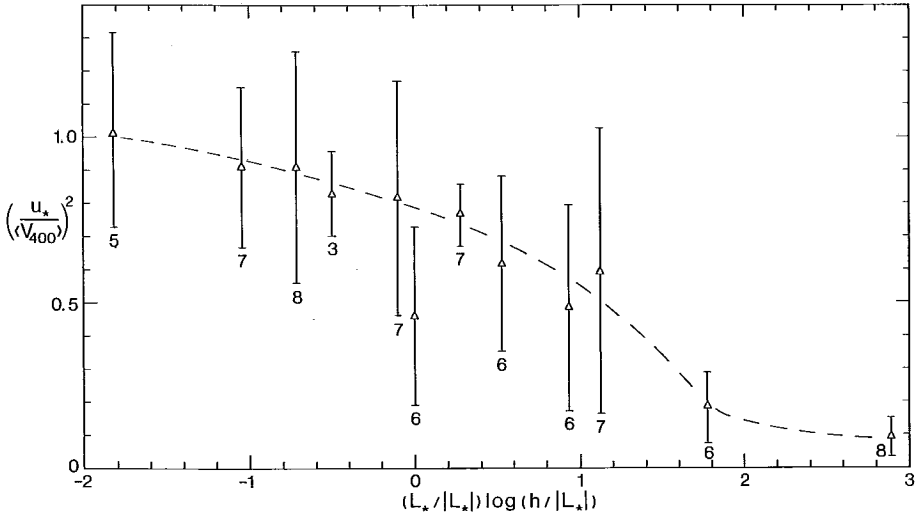

Fig. 5. Same as Fig. 4 but for $(u_*/\langle V_{400}\rangle)^2$.

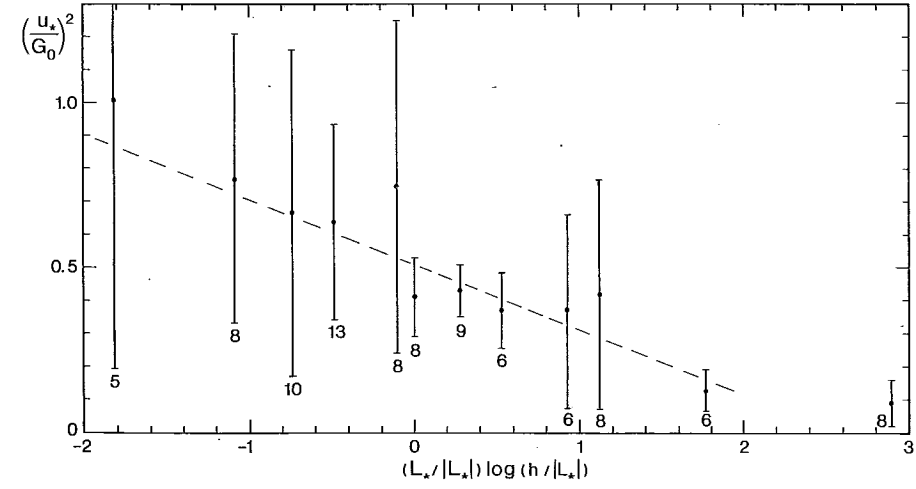

Fig. 6. Same as Fig. 4 but for $(u_*/G_0)^2$.

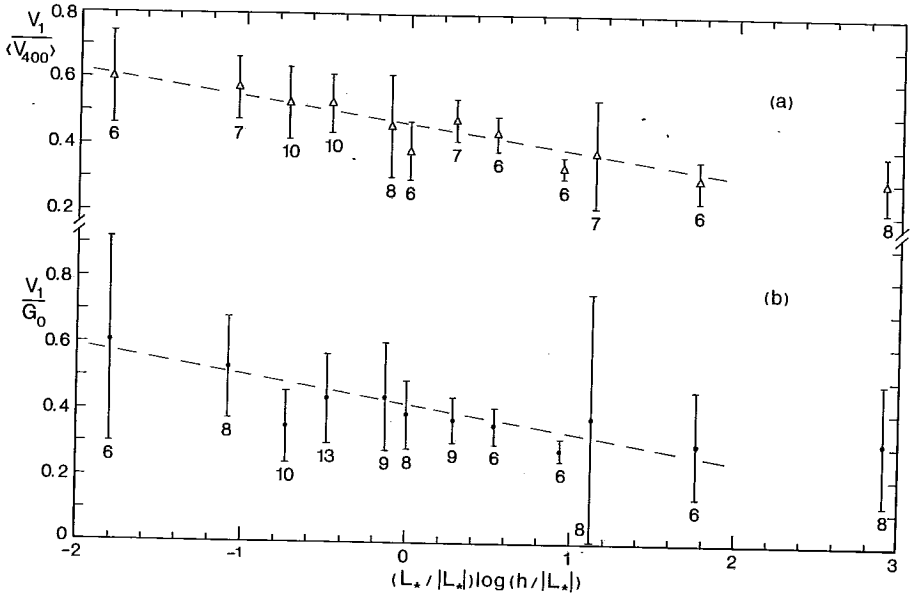

Fig. 7. Same as Fig. 4 but for a) $V_1/\langle V_{400}\rangle$ and b) V_1/G_0.

to play any role. From our experimental data, we can take the lowest observable level, namely 1 m. Such minimum wind V_1 is not intended for practical purposes but as an intermediate tool for forecasting purposes.

From HICKS (1976) and JOFFRE (1982) we know that there is a well-defined linear relationship between V_1 and $u_\star$. The only curvature appearing at very low velocity is due to wake effects of roughness elements and inaccuracies in measuring $u_\star$ at low signal levels. The dependence of the wind ratio $R_1 = V_1/V_{up}$ on stability is shown in Figs. 7a and 7b for $V_{up} = \langle V_{400}\rangle$ and G_0, respectively. The expected decreasing trend from unstable to stable cases occurs here, too. Note that this decrease is much smoother than in the previous figures and the departure from the figured trend is very small. The standard deviations of the stability groups are also smaller and much smaller in the $\langle V_{400}\rangle$ case.

Thus, referring to our premises that we are looking for simple statistical-dynamical predictors implicitly incorporating stability effects, we can summarize the above results by pointing out the advantage of using the lower wind V_1 and the global driving wind $\langle V_{400}\rangle$.

3.2 Theoretical considerations

In principle, G_0, which is obtained from the surface pressure field, contains only the large-scale dynamical forcing while the vertically integrated mean boundary layer wind $\langle V \rangle$ also contains such effects as thermal stability and baroclinicity.

We can theoretically compare these two terms. Let us start from the steady state equations of motion, integrated vertically from the surface to the ABL height h, assuming no fluxes at h and choosing the x-axis along the surface stress. Then,

$$\langle u \rangle = u_{g0} + \frac{1}{2} S_u h \tag{3}$$

$$\langle v \rangle = v_{g0} + u_\star^2/hf + \frac{1}{2} S_v h \tag{4}$$

with $\langle V \rangle = (\langle u \rangle^2 + \langle v \rangle^2)^{1/2}$ and $G_0 = (u_{g0}^2 + v_{g0}^2)^{1/2}$, while $S_u = \partial u_g/\partial z$ and $S_v = \partial v_g/\partial z$ are the vertical geostrophic shear components above the ABL. In the first approximation let us neglect the baroclinic effects so that

$$\langle V \rangle^2 = G_0^2 + \frac{u_\star^2}{hf}(2v_{g0} + u_\star^2/hf) \tag{5}$$

Introducing the geostrophic drag coefficient C_g and the cross isobaric angle α_0 between G_0 and τ_0, we obtain

$$(\langle V \rangle/G_0)^2 = 1 + C_g^{1/2}(2\sin\alpha_0 + C_g^{1/2}/h_\star)\, h_\star^{-1} \tag{6}$$

where $h_\star = h/L_E$ ($L_E = u_\star/f$) is the height ratio. The terms C_g and $\sin\alpha_0$ can be expressed using the resistance laws (*e.g.* ARYA, 1977) and

$$\frac{\langle V \rangle^2}{G_0^2} = 1 + \frac{(0.16\, h_\star^{-1} - 0.8a)\, h_\star^{-1}}{[\ln(h/z_0) - b]^2 + a^2} \tag{7}$$

where a and b are the two universal dimensionless functions of the general similarity theory for the ABL depending on the two parameters $\mu_h = h/L_\star$ and $h_\star = h/L_E$. Empirical data on these two functions produce a large scatter so that their analytical form is not well known. However, ARYA (1977, 1978) derived the best available expressions for a and b based on ABL modelling results. From his results, the ratio $F = \langle V \rangle/G_0$ can be computed as a function of stability and of the height ratio $h_\star$. This is shown in Fig. 8 for unstable and stable conditions

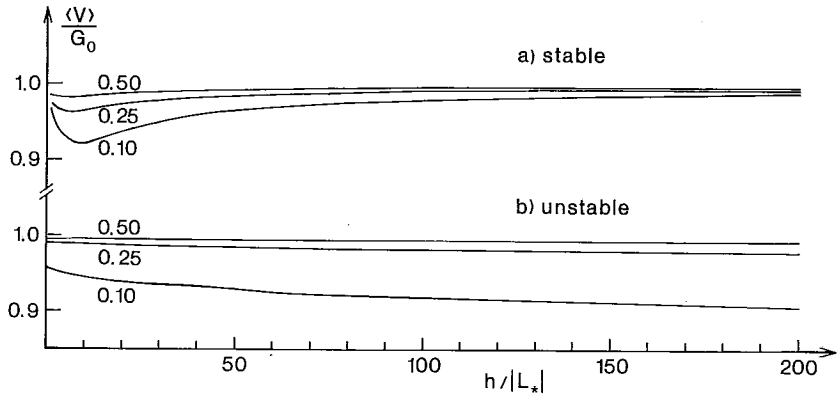

Fig. 8. Theoretical dependence of the ratio $\langle V_{400}\rangle/G_0$ on thermal stability for (a) stable and (b) unstable cases.

separately. In the computations we took h = 400 m while $z_0 = Z_0$ = 0.08 cm, Z_0 being the large-scale overall roughness parameter (see JOFFRE, 1983).

We note that the ratio F is more or less independent of stability except in near-neutral conditions. The appearance of the F curve close to neutrality is also influenced by the analytical form of the expressions for a and b, which interpolate between neutral and convective conditions or between neutral and very stable conditions. There is no justification for such variability; on the contrary, F should be a continuous function when shifting from one type of stability to the other through neutral conditions. Note that $h_\star$ is important only for low $h_\star$ values under unstable conditions. These curves show that $\langle V\rangle$ is a good approximation for the large-scale flow taking into account stability effects in a smooth way.

4. *Dynamical-statistical wind predictions*

4.1 The model

The local surface wind over a given area can be predicted in two alternative ways: either with a more or less detailed numerical model of the ABL in which the structure of the flow is simulated and boundary conditions are imposed, or with a statistical model in which the unknown parameters are related to available predictors and where the numerical coefficients are derived from a suitable data base. Although the closure problem and finite difference approximations may alter the results the first approach is in principle the best. Furthermore, a far larger

number of boundary conditions is required if the degree of accuracy of the results is to be at the level of the degree of complication of the model.

The simplest approach of a statistical model using one or more suitable predictors explaining, let us hope, most of the variations in the considered parameter might then be more relevant in certain cases. Better accuracy could obviously be achieved by considering several predictors, but, it is not always easy to extract the isolated influence of each parameter from data sets. On the basis of the previous results, let us choose here the quantity $\langle V_{400} \rangle$ as the main predictor for the surface wind since it is closely related to G_0, the main external driving force, and it is little affected by stability. We shall refer to this model by the denomination BULK.

The procedure whereby the statistical equations of the model are derived is first to estimate $\langle V_{400} \rangle$ as a fixed fraction of G_0 and then to compute V_{10} from $\langle V_{400} \rangle$ (see Fig. 9). This figure reveals that the distinction between different stability cases does not classify the data any better. Moreover, it is difficult to derive a stability index from routine observations or a general circulation model like the filtered model of the FMI. Thus, no explicit distinction between stability classes will be made.

Since $\langle V_{400} \rangle$ is derived from G_0, we could have derived V_{10} (or V_1) directly from G_0. The dependence of V_{10} on G_0 illustrated in Fig. 10 explains partially why we did not do so: the scatter is much larger than in Fig. 9.

The surface wind direction was determined using the mean ABL wind direction α_m defined as

$$\alpha_m = \tan^{-1} (\langle v_{400} \rangle / \langle u_{400} \rangle) \tag{8}$$

This cross-isobaric angle is weighted statistically using the observed values and corrected with a constant turning of 22°.

The geostrophic wind derived from the pressure field showed a positive lag of several hours compared with the observed surface wind (see §4.2). This effect was compensated by imposing a delay of 6 hrs when the wind velocity and wind direction changes rapidly, *i.e.* at the approach of a low-pressure system.

On the other hand, an earlier statistical surface wind prediction model has been developed at the FMI (LANGE, 1973). The model is based on prediction from a 6-layer filtered model with correction from wind statistics to allow for seasonal, orographic and mesoscale factors. Moreover, persistency is accounted for with iterative techniques. The Gulf of Bothnia is divided into four regions and wind predictions are put out every six hours for each of these regions (see Fig. 1). We shall refer to it as LOCWI.

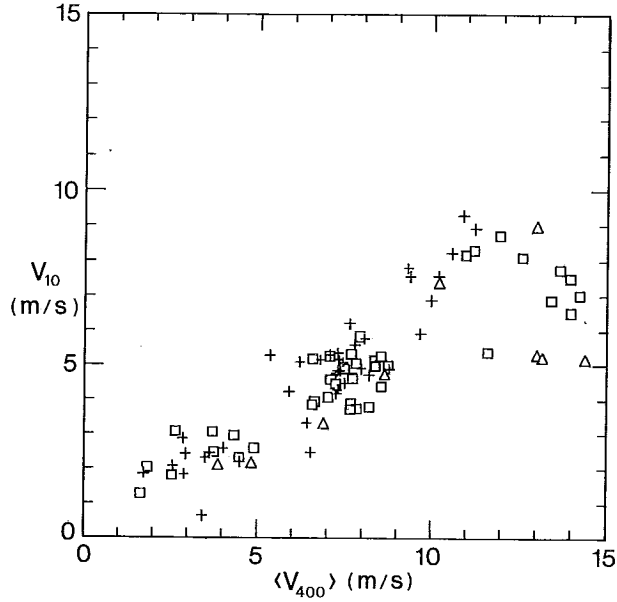

Fig. 9. Scatter diagram between the observed surface wind V_{10} and the vertically averaged wind $\langle V_{400} \rangle$. Distinction is made between stable cases (squares), near-neutral cases (triangles) and unstable cases (crosses).

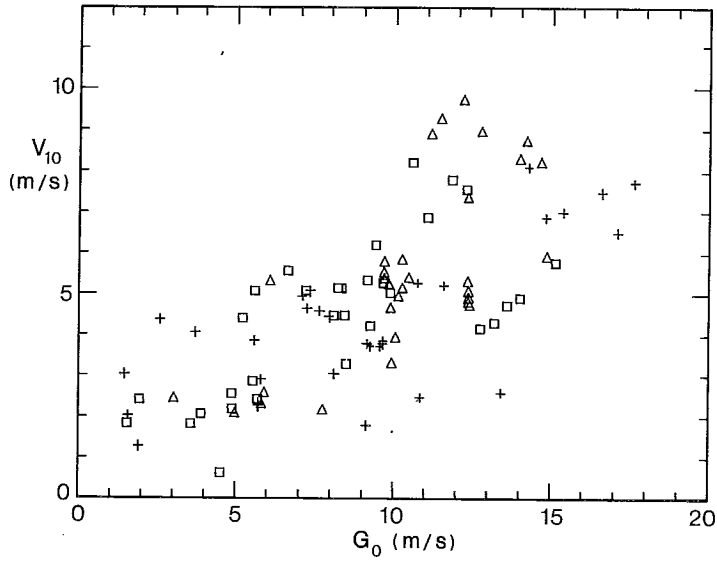

Fig. 10. Same as Fig. 9 but for V_{10} vs. G_0.

4.2 Comparison of predicted surface winds with observations

Let us define the fractional error as

$$\sigma_u = 100 \frac{u_{prd} - u_{obs}}{\frac{1}{2}(u_{prd} + u_{obs})} \tag{9}$$

to estimate the deviation between the predicted u_{prd} and the observed quantity u_{obs}. The advantage of this quantity is that it is logarithmically unbiased, *i.e.* a predicted value which is k times the measured value produces numerically the same fractional error as a predicted value which is $1/k$ of the measured value.

The predictions from both statistical models should be compared with an independent data base. For that we use the surface wind observations at 6 hr intervals during the three weeks of the experiment. The results are shown in Figs. 11 and 12 for the two experimental sites, respectively. With our BULK

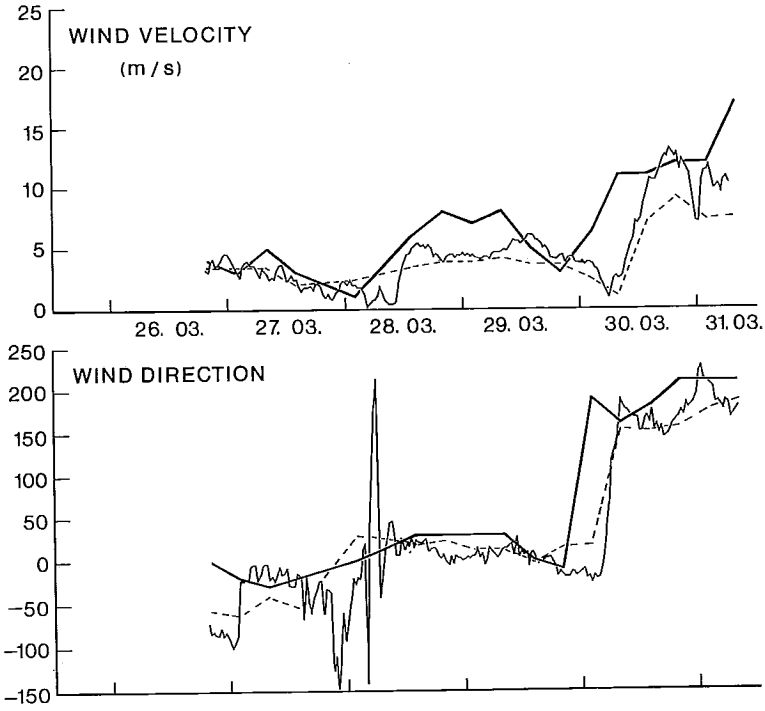

Fig. 11. Comparison of predicted surface wind velocity and direction from the BULK method (dashed line) with the observed wind quantities (thin continuous line) and the LOCWI wind predictions (bold line) for the F1 phase.

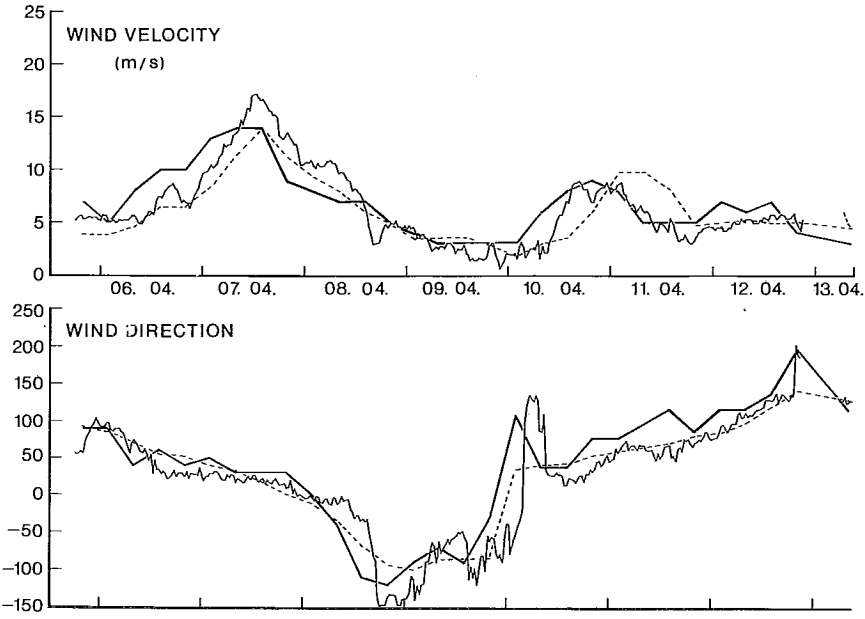

Fig. 12. Same as Fig. 11 but for the F2 phase.

model based on vertically averaged wind we obtain,

$$\sigma = (-19.5 \pm 27)\ \% \quad \text{for F1}$$

$$\sigma = (-\ 2.1 \pm 25)\ \% \quad \text{for F2}$$

while for the local surface wind LWW obtained from the LOCWI model we get

$$\sigma = (23.5 \pm 43)\ \% \quad \text{for F1}$$

$$\sigma = (\ 9.2 \pm 28)\ \% \quad \text{for F2}$$

where F1 and F2 refer to the March and April periods, respectively. Note the smaller absolute values of σ for the BULK model. Moreover, its smaller standard deviation indicates that, on the average, wrong forecasts are less serious than when using the LOCWI forecasts. It is noteworthy that predictions from LOCWI correspond to an overestimation of the surface wind ($\sigma > 0$). The negative values of the fractional error for the BULK predictions indicate that these underestimate the observed wind, particularly during maximum wind periods. This may be because mesoscale effects are not taken into consideration in the model. In that sense, by emphasizing local accelerations, a third-order regression fit to the surface pressure

field might give better results than our second-order fit. A more likely reason for this underestimation of strong wind cases is the bias in the data towards moderate wind conditions, since severe wind conditions or stormy weather prevented us from performing profile observations and thus these interesting conditions were not included in the statistics used to implement the BULK model.

Although the LOCWI prediction model contains seasonal and other Fourier components, the results would have been similar had the surface wind only been taken as a fixed fraction of the geostrophic wind. For the sample of 47 observations at 6 hr intervals we find $\overline{(\mathrm{LWW}/G_0)} = 0.80 \pm 0.39$. The correlation between the geostrophic wind obtained from the surface pressure field analysis and the local wind LWW is 0.79 for the whole data set. The overall correlation coefficient between the observed surface wind and the BULK model products is 0.90 whereas it is only 0.79 for the local wind LWW.

As to the wind direction WD, the mean absolute error is

$$\Delta\mathrm{WD} = -1^\circ \pm 27^\circ \quad \text{for F1}$$

$$\Delta\mathrm{WD} = 1.5^\circ \pm 28^\circ \quad \text{for F2}$$

whereas for the local wind direction LWD we get

$$\Delta\mathrm{LWD} = 26.5^\circ \pm 53^\circ \quad \text{for F1}$$

$$\Delta\mathrm{LWD} = 11.8^\circ \pm 40^\circ \quad \text{for F2}$$

where $\Delta\mathrm{WD} = \mathrm{WD}_{prd} - \mathrm{WD}_{obs}$. Here again the predictions based on the bulk angle α_m (see Eq. 8) are much better on the average and provide smaller standard deviations, whereas the very large standard deviations for LWD imply a very bad prognosis in certain cases.

A noteworthy feature is the forward shift of the LOCWI wind together with the geostrophic wind V_{g0} with respect to observations noticeable at the start of unstationary periods (low pressure systems sweeping over the site). The wind increase or the change in wind direction are by and large predicted to start about 6–9 hrs before they are observed. This time shift is of necessity a rough value since predictions are only available every six hours. This may imply that the group velocity of the disturbance is smaller than the phase velocity, thus indicating that the particular waves were not of the Rossby type. It also implies that the derivative of the phase velocity with respect to wave length is positive, *i.e.* the phase velocity of the particular wave is an increasing function of the wavelength. However, further comparison between the same statistically predicted local wind and the surface wind observed at automatic stations (in January–May 1979) did not show similar

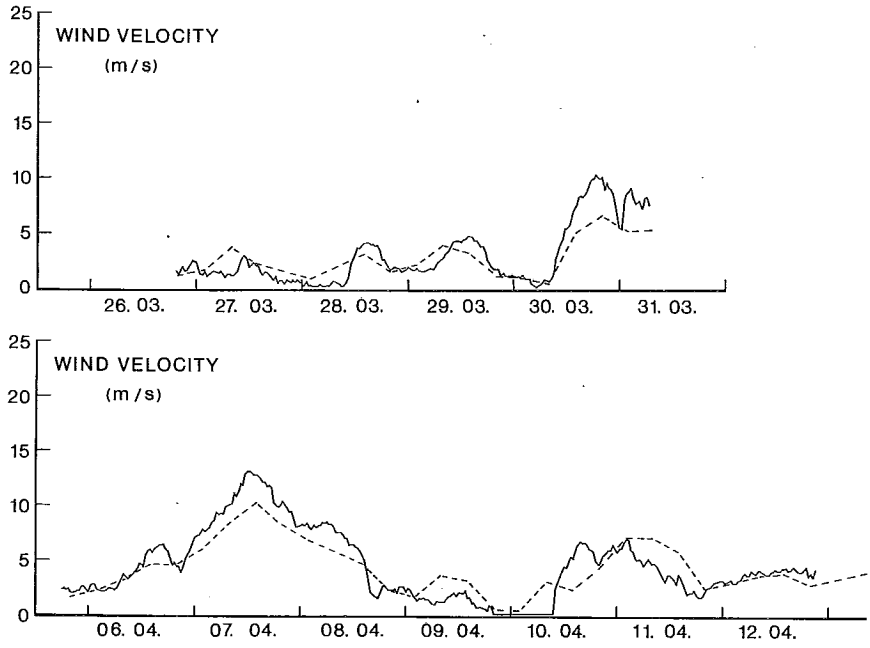

Fig. 13. Comparison of predicted 1 m winds from the BULK model (dashed line) with the observed wind at 1 m (continuous line).

systematic behaviour although it was apparent from time to time. This indicates that the observed feature, if real, is connected to a specific type of circulation; otherwise it is a sampling error.

The 1 m wind was predicted in the same way from the BULK model. The results are shown in Fig. 13. Here, too, the overall correlation is 0.90 whereas the fractional error is (-3 ± 45) % for F1 and (11.5 ± 53) % for F2, respectively. To obtain these predictions, however, a diurnal cycle component was introduced in order to reproduce the diurnal oscillation of the period March 27–29 when the large-scale flow was weak. The amplitude A of the cycle was modulated in the following way

$$A = \frac{A}{1 + G_0^4} \tag{10}$$

so that the cycle disappears when G_0 becomes large.

5. *Conclusions*

In this preliminary study, we have shown that the non-classical wind concept of vertically-averaged mean wind can act as a good predictor of surface wind velocity and direction over sea areas, regardless of stability conditions. The lower correlation (or larger scatter) under stable conditions indicates that either the mean ABL height of 400 m, corresponding roughly to the 950 mb level, is not adequate and that the upper level of integration should be lowered to, say, 200 m, or that the surface pressure field approach, which constitutes the first step of the forecast procedure is not relevant under very stable conditions when the different layers of the lower atmosphere are poorly coupled. The former deficiency might be compensated by the fact that in general the windshear increases as the height of the ABL decreases with increasing stability, so that the term $\langle V_h \rangle$ should be more or less conserved. In contrast, the latter deficiency has also been observed in trajectory computations of long-range transport (SMITH, 1982) and an upper level driving flow (*e.g.* 900 or 850 mb) should be used instead.

The results of the method presented here are encouraging enough to incorporate additional observation data in the statistical regression and thus to extend the applicability of the method. This is under way with the data of a second large field experiment.

Acknowledgements: The financial support of the Board of Navigation is gratefully acknowledged.

REFERENCES

ARYA, S.P.S., 1977: Suggested revisions to certain boundary layer parameterization schemes used in atmospheric circulation models. *Monthly Wea. Rev.*, **105**, 215–227.

–»–, 1978: Comparative effects of stability, baroclinity and the scale-height ratio on drag laws for the atmospheric boundary layer. *J. Atmos. Sci.*, **35**, 40–46.

HICKS, B.B., 1976: Wind profile relationships from the Wangara Experiment. *Quart. J. R. Meteor. Soc.*, **102**, 535–551.

JOFFRE, S.M., 1981: The physics of the mechanically-driven atmospheric boundary layer as an example of air-sea ice interactions. *Univ. of Helsinki, Dept. of Meteorology, Rep. No. 20*, 75 pp.

–»–, 1982: Momentum and heat transfers in the surface layer over a frozen sea. *Boundary-Layer Meteorol.*, **24**, 211–229.

–»–, 1983: Determining the form drag contribution to the total stress of the atmospheric flow over ridged sea ice. *J. Geophys. Res.*, **88**, C7, 4524–4530.

LANGE, A., 1973: Statistical surface wind prediction in Finland. *Finnish Meteorological Institute, Techn. Report No. 6*, 23 pp.

LETTAU, H.H., 1959: Wind profile, surface stress and geostrophic drag coefficients in the atmospheric surface layer. *Adv. in Geophys.*, 6, Ed. by F. Frenkiel & P.A. Sheppard, Acad. Press, 241–257.

MONIN, A.S. and A.M. YAGLOM, 1971: *Statistical Fluid Mechanics.* 1, Ed. by J. Lumley, the M.I.T. Press, 769 pp.

SMITH, F.B., 1982: Transport processes and meteorological factors. *W.M.O. Technical Note No. 177,* 11–32.